Study of Excited Ξ^- Baryons in $\bar{p}p$-Collisions with $\overline{\mathrm{P}}$ANDA

Authors:

Jennifer Pütz, Albrecht Gillitzer, James Ritman

Contents

1 Introduction

Understanding the excitation pattern of baryons is indispensable for a deep insight into the mechanism of non-perturbative QCD. Up to now only the nucleon excitation spectrum has been subject to systematic experimental studies while very little is known on excited states of double or triple strange baryons.

In studies of antiproton-proton collisions the $\overline{\mathrm{P}}$ANDA experiment is well-suited for a comprehensive baryon spectroscopy program in the multi-strange and charm sector. A large fraction of the inelastic $\bar{\mathrm{p}}\mathrm{p}$ cross section is associated to final states with a baryon-antibaryon pair together with additional mesons, giving access to excited states both in the baryon and the antibaryon sector.

In the present study we focus on excited Ξ^- states. For final states containing a Ξ^- $\bar{\Xi}^+$ pair cross sections up to the order of μb are expected, corresponding to production rates of $\sim 10^6$/d at a Luminosity $L = 10^{31}\,\mathrm{cm}^{-2}\,\mathrm{s}^{-1}$ (5% of the full value). A strategy to study the excitation spectrum of Ξ^- baryons in antiproton-proton collisions will be discussed. The reconstruction of reactions of the type $\bar{\mathrm{p}}\mathrm{p} \to \Xi^{-*}\bar{\Xi}^+$ (and their charge conjugate) with the $\overline{\mathrm{P}}$ANDA detector will be presented based on a selected exemplary reaction and decay channel.

2 Event generation

To study excited Ξ^- baryons the simulation of a sufficient number of signal events is needed. For this study 1.5 million signal events were generated with the event generator EvtGen. The reaction and decay tree selected for the simulation is shown in figure 2.1. If not otherwise specified, the charged conjugate process is implicitly included in the following.

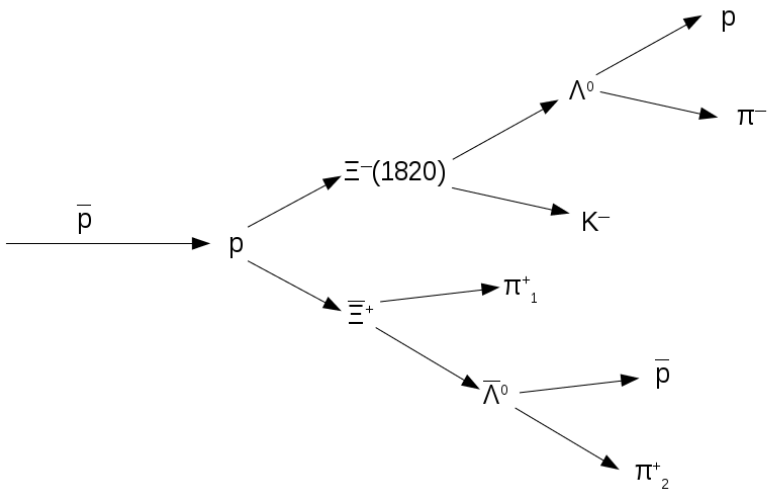

Figure 2.1: Reaction and decay tree selected for the simulation.

For the charge conjugate channel another 1.5 million events were generated. Table 2.1 shows the parameters used for the event generation.
For the production reaction $\bar{\mathrm{p}}\mathrm{p} \to \Xi^-(1820)\,\bar{\Xi}^+$ the PHSP model, generating an isotropic angular distribution, was used, because a more realistic treatment has not yet been implemented in EvtGen. This simplification does not affect the strategy used for this study.
The chosen beam momentum $p_{\bar{\mathrm{p}}} = 4.6\,\mathrm{GeV/c}$ corresponds to a center-of-mass energy of 100

Table 2.1: Parameter for event generation

Parameter	Value
Beam momentum	4.6 GeV/c^2
Production	PHSP
Tracking	Ideal
Particle ID	Ideal

Table 2.2: Used software version

Software	Version
FairSoft	mar15
FairRoot	v-15.03a
PandaRoot	trunk revision 28555
Geant	3
Genfit	1

MeV above the production threshold of Ξ^- (1820) and $\bar{\Xi}^+$. The production cross section is expected to be of the same order ($\sim \mu$b) as for ground state Ξ^- production in $\bar{p}p \to \Xi^- \bar{\Xi}^+$ [1]. This expectation is based on ground state and excited state single strange hyperons production data in $\bar{p}p$ collisions [2].

The used software version for PandaRoot and the external software package is listed in table 2.2.
The missing Ξ^- (1820) was defined in the evt.pdl file listing the properties of particles used in EvtGen. The properties of Ξ^- (1820) are listed in table 2.3.

Table 2.3: Properties of Ξ^- (1820) and $\bar{\Xi}^+$ (1820). The values are taken from [3]

Particle	J	I	P	Charge	Mass	Width
Ξ^- (1820)	$\frac{3}{2}$	$\frac{1}{2}$	(-1)	(-1)	(1.823 ± 5) GeV/c^2	(0.024 ± 6) GeV/c^2
$\bar{\Xi}^+$ (1820)	$\frac{3}{2}$	$\frac{1}{2}$	(-1)	1	(1.823 ± 5) GeV/c^2	(0.024 ± 6) GeV/c^2

The generated transverse momentum versus the longitudinal momentum for Λ and $\bar{\Lambda}$ is presented in figure 2.2 and for $\bar{\Xi}^+$ and Ξ^- (1820) in figure 2.3.

Figure 2.4 shows the Dalitz plot for the Λ, K^- and $\bar{\Xi}^+$ final states for the channel $\bar{p}p \to \Xi^-$ (1820) $\bar{\Xi}^+$.

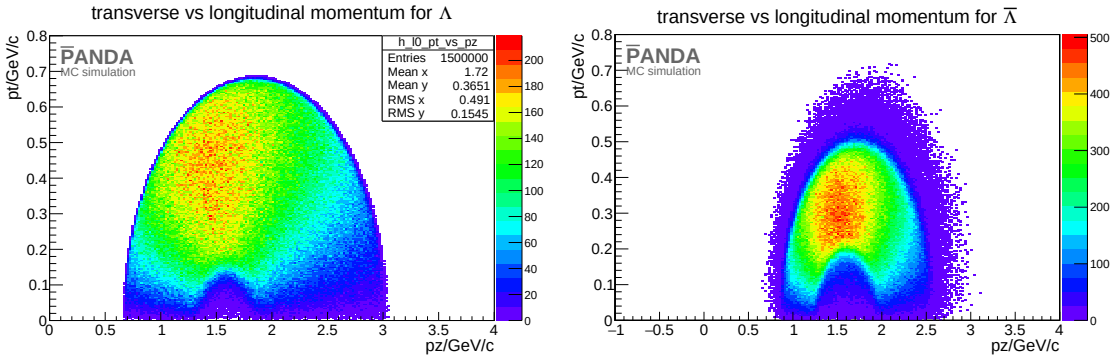

(a) Λ (b) Λ̄

Figure 2.2: "PROPOSED FOR RELEASE" Figure a) shows the transverse momentum on the y axis versus the longitudinal momentum on the x axis for Λ. Figure b) shows the same distribution for Λ̄.

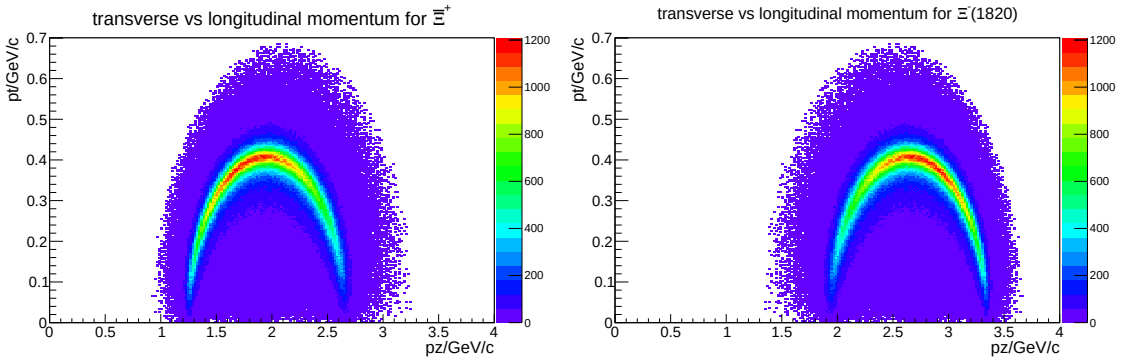

(a) Ξ̄+ (b) Ξ− (1820)

Figure 2.3: "PROPOSED FOR RELEASE" Figure a) shows transverse versus the longitudinal momentum distribution for Ξ̄+. Figure b): transverse versus longitudinal momentum distribution for Ξ− (1820).

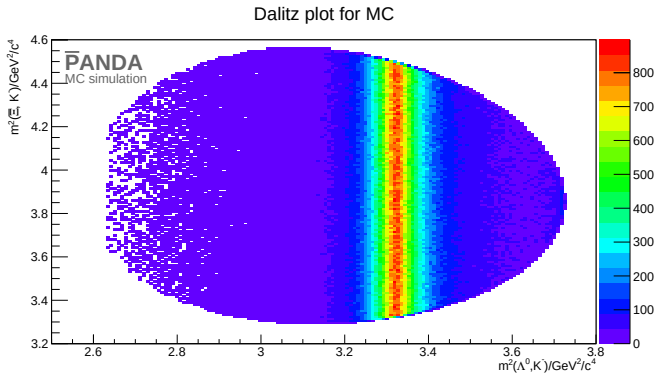

Figure 2.4: "PROPOSED FOR RELEASE" $\bar{\Xi}^+$ Λ K^- dalitz plot for generated events is shown. On x axis is the squared mass of Λ K^- system and on the y axis there is the squared mass of $\bar{\Xi}^+$ K^- system.

3 Analysis

To reconstruct all the particles involved in the reaction we start with the final state particles and go backwards through the reaction chain.

3.1 Final state particles

The selected final state particle are protons, anti-protons, π^-, π^+, K^- and K^+ mesons. For the reconstruction of these particles an ideal tracking was used. Ideal tracking means that the hit points caused by a particle track are grouped based on the generated particle information. To achieve a more realistic reconstruction efficiency only particles with more than 3 hits in any inner tracking detector (MVD, STT and GEM) are selected. The selection criterion is chosen because three hits are needed to defining a circle. A fourth hit point is then a validation of the track hypothesis.
The particle identification (PID) is also ideal meaning that the true particle gets the probability $P = 1$, the others $P = 0$. The selection criterion is set to 'best'.

The reconstruction efficiency and the momentum resolution for the final state particle is shown in table 3.1 and figure 3.1. All reconstruction efficiencies are calculated with the MC matched particles.
Table 3.2 shows the reconstruction efficiency and the momentum resolution for the charge conjugate channel.

Table 3.1: "PROPOSED FOR RELEASE" Reconstruction efficiency and momentum resolution for $\bar{p}p \to \Xi^-(1820)\,\bar{\Xi}^+$

final state	N/%	$\frac{\sigma p}{p}$/%
π^-	83.48	1.53
π_1^+ ($\bar{\Xi}^+$)	80.93	1.38
π_2^+ ($\bar{\Lambda}$)	83.07	1.49
K^-	78.59	1.58
p	84.39	1.61
$\bar{p}$	78.25	1.61

Table 3.2: "PROPOSED FOR RELEASE" Reconstruction efficiency and momentum resolution for $\bar{p}p \to \bar{\Xi}^{+}(1820)\,\Xi^{-}$

final state	N/%	$\frac{\sigma p}{p}$/%
π^{+}	82.96	1.54
π_1^{-} (Ξ^{-})	80.40	1.38
π_2^{-} (Λ)	82.69	1.49
K^{+}	83.27	1.58
p	80.71	1.55
$\bar{p}$	80.93	1.60

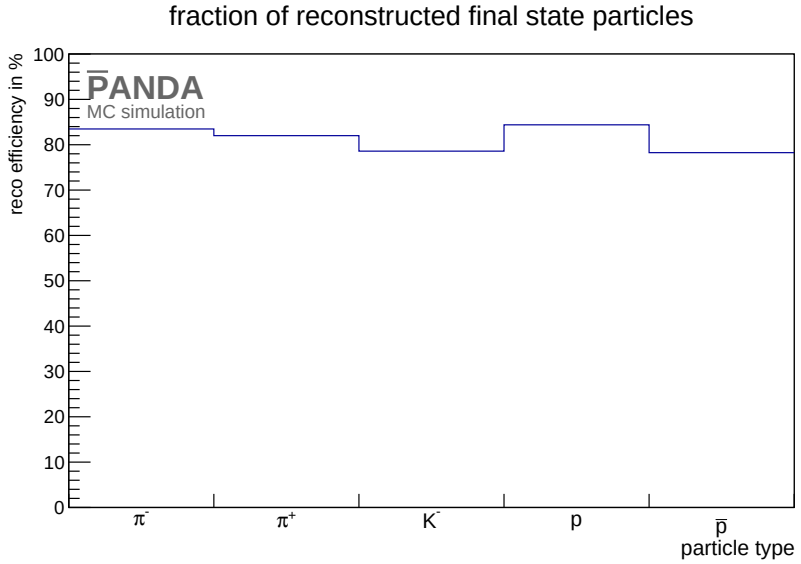

Figure 3.1: "PROPOSED FOR RELEASE" Reconstruction efficiency for final state particles. The x axis shows the particle type. On the y axis the fraction of reconstructed particles is shown.

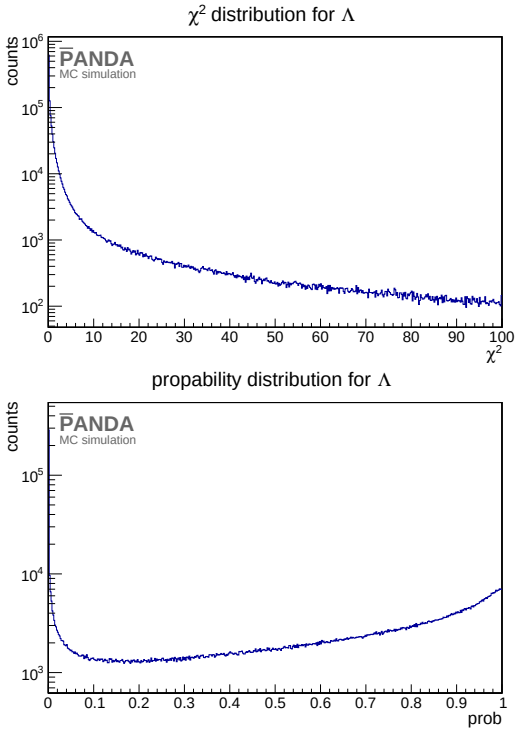

Figure 3.2: "PROPOSED FOR RELEASE" The upper plot shows the χ^2 distribution and the lower plot shows the probability distribution for the Λ vertex fit.

3.2 Reconstruction of Λ and $\bar{\Lambda}$

Selection

For the reconstruction of Λ hyperons a proton and a π^- meson are combined and for the reconstruction of $\bar{\Lambda}$ a $\bar{\mathrm{p}}$ and a π^+ are combined. After combining the daughter particles a mass cut is performed. Only those candidates are chosen which have a mass within a window of $0.3\,\mathrm{GeV/c^2}$ symmetric to the nominal Λ mass, i.e., a mass within $M = 1.116 \pm 0.15\,\mathrm{GeV/c^2}$.

A vertex constraint fit with the PndKinVtxFitter is performed on the selected candidate. This means that the tracks of the daughter particles are fitted to a common vertex point. The χ^2 and probability distribution of the vertex fit for Λ candidates is shown in figure 3.2.

In the probability distribution one can see an increasing number of events for probabilities approaching a value of one. This feature is not the vertex fit itself, as was shown by tests based on the so-called "poormantrack" algorithm [4].

A mass contraint fit is performed on the fitted candidate. For this mass constraint fit the

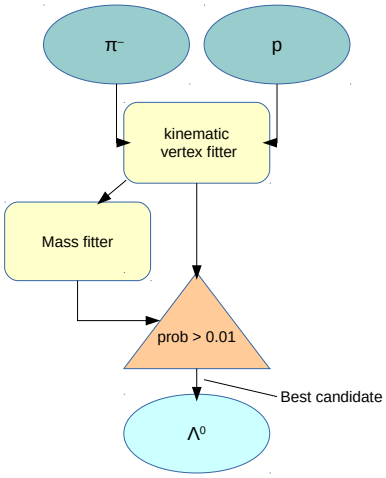

Figure 3.3: "PROPOSED FOR RELEASE" Scheme for Λ reconstruction

kinematic fitter PndKinFitter is used. After using both fitters the selection criterion is set. One select only those particles which have a probability larger than 1% in both fitter. A scheme which shows how the events are selected can be found in figure 3.3.
If there is more than one candidate left after these cuts, the candidate with the lowest χ^2 is chosen.

Results

In this paragraph the Λ and $\bar{\Lambda}$ sample obtained with the chosen selection criteria is presented. The mass distributions correspondingt to the different cuts are shown in figure 3.4 and figure 3.5 for Λ and $\bar{\Lambda}$, respectively.
The reconstructed mass can be determined by performing a double Gaussian fit on the mass distribution obtained after all cuts. The mass distribution and the double Gaussian fit are shown for Λ candidates in figure 3.6.
The peak position of the Gaussian fit is taken as the value of the reconstructed mass. The reconstructed masses are $m_{\Lambda^0} = (1.1158 \pm 0.0022)\,\mathrm{GeV/c^2}$ and $m_{\bar{\Lambda}^0} = (1.1159 \pm 0.0022)\,\mathrm{GeV/c^2}$ for Λ and $\bar{\Lambda}$, respectively. Figure 3.7 shows the transverse momentum versus the longitudinal momentum.
After all cuts the reconstruction efficiency is 50.33% for Λ and 41.46% for $\bar{\Lambda}$. The difference

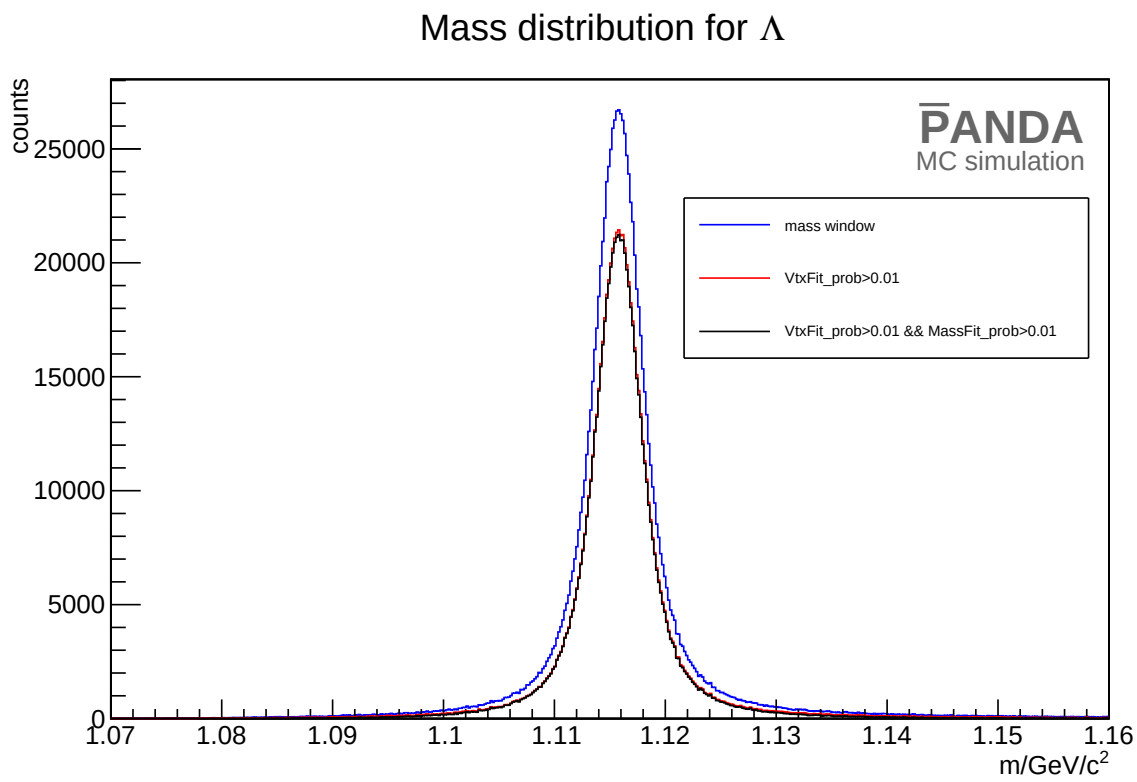

Figure 3.4: "PROPOSED FOR RELEASE" Mass distribution of Λ after the mass cut (blue), after the vertex fit cut (red) and after all cuts (black).

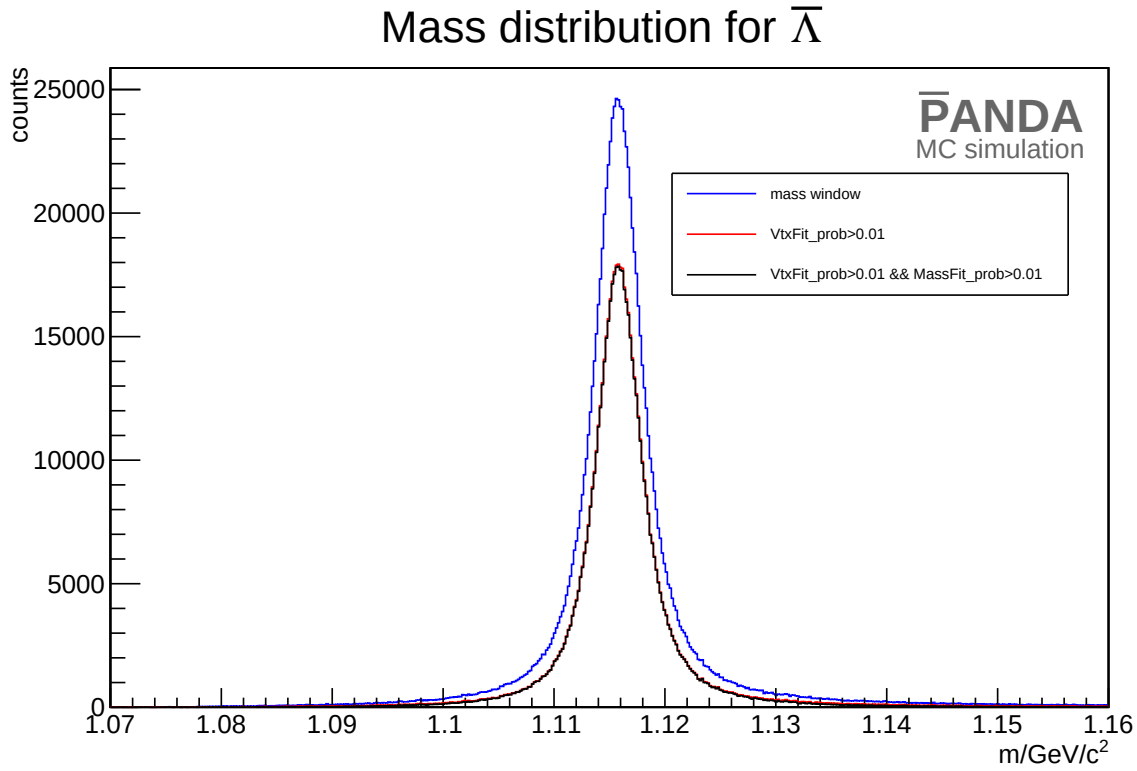

Figure 3.5: "PROPOSED FOR RELEASE" Mass distribution of $\bar{\Lambda}$ after the mass cut (blue), after the vertex fit cut (red) and after all cuts (black).

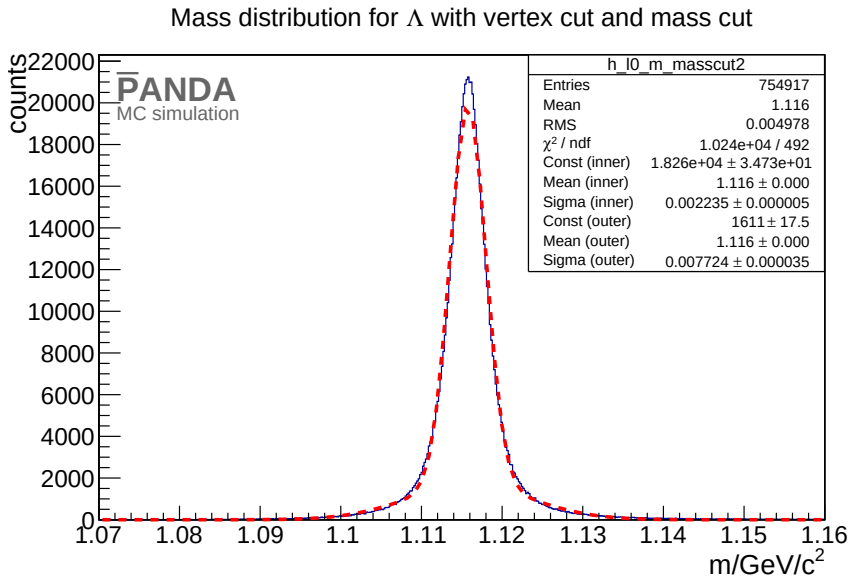

Figure 3.6: "PROPOSED FOR RELEASE" Mass distribution (blue histogram) for Λ fitted with a double Gaussian fit (red dashed line).

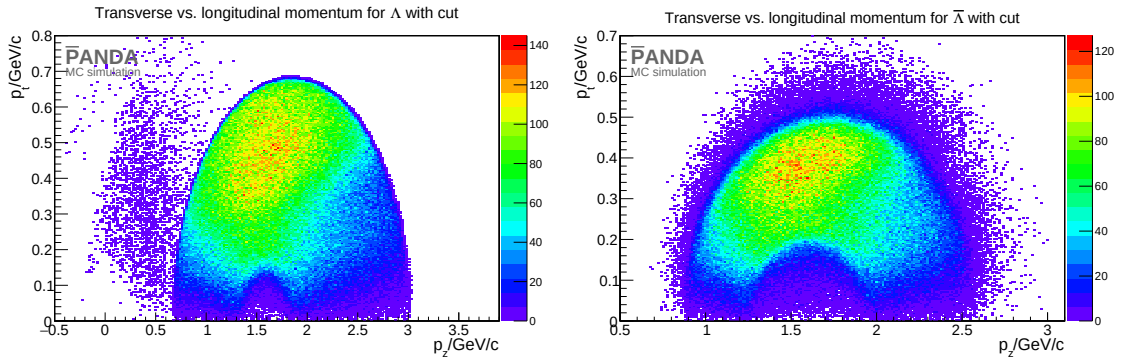

(a) (b)

Figure 3.7: "PROPOSED FOR RELEASE" Figure a): transverse versus longitudinal momentum for Λ. Figure b):transverse versus longitudinal momentum for $\bar{\Lambda}$.

in the reconstruction efficiencies for Λ and $\bar{\Lambda}$ is caused by the different decay lengths of their mother particles. Λ is emitted by the Ξ^- (1820) which has a very short decay length while the decay length of $\bar{\Xi}^+$ is $c\tau = 4.91\,\text{cm}$ [3]. The decay length of Λ and $\bar{\Lambda}$ is $c\tau = 7.98\,\text{cm}$, so that the final state particles of $\bar{\Lambda}$ are produced more downstream than the final state particles of Λ. This can be also seen in figure 3.8. The finale state particles of $\bar{\Lambda}$ are produced at the edge of the MVD detector so that the reconstruction efficiency for these particles is reduced.

3.3 Reconstruction of Ξ^- and $\bar{\Xi}^+$

Selection

The reconstruction of Ξ^- and $\bar{\Xi}^+$ follows a similar scheme like the reconstruction of Λ and $\bar{\Lambda}$. For $\bar{\Xi}^+$ are $\bar{\Lambda}$ and π_1^+ recombined and for Ξ^- in the charge conjugate. channel Λ and π_1^-. Now it is distinguished between the to π^+ (π^-) particle and use only those particles which have not already been combined. After combining the daughter particles a mass window cut is performed with a width of $0.3\,\text{GeV/c}^2$ around the Ξ^- mass $m_\Xi = 1.32171$ GeV/c^2 [3].

The fitting scheme is the same as for Λ and $\bar{\Lambda}$ and is shown in figure 3.9 After the mass window cut the daughter particles are fitted to a common vertex with the PndKinVtxFitter. And again these information is used to perform the mass constraint fit.

Only those particles are selected which have a χ^2 probability of more than 1 % in both fitter. Figure 3.10 shows exemplarily the cut on the vertex fit probability.

If there is more than one candidate left after all cuts, the best candidate is chosen.

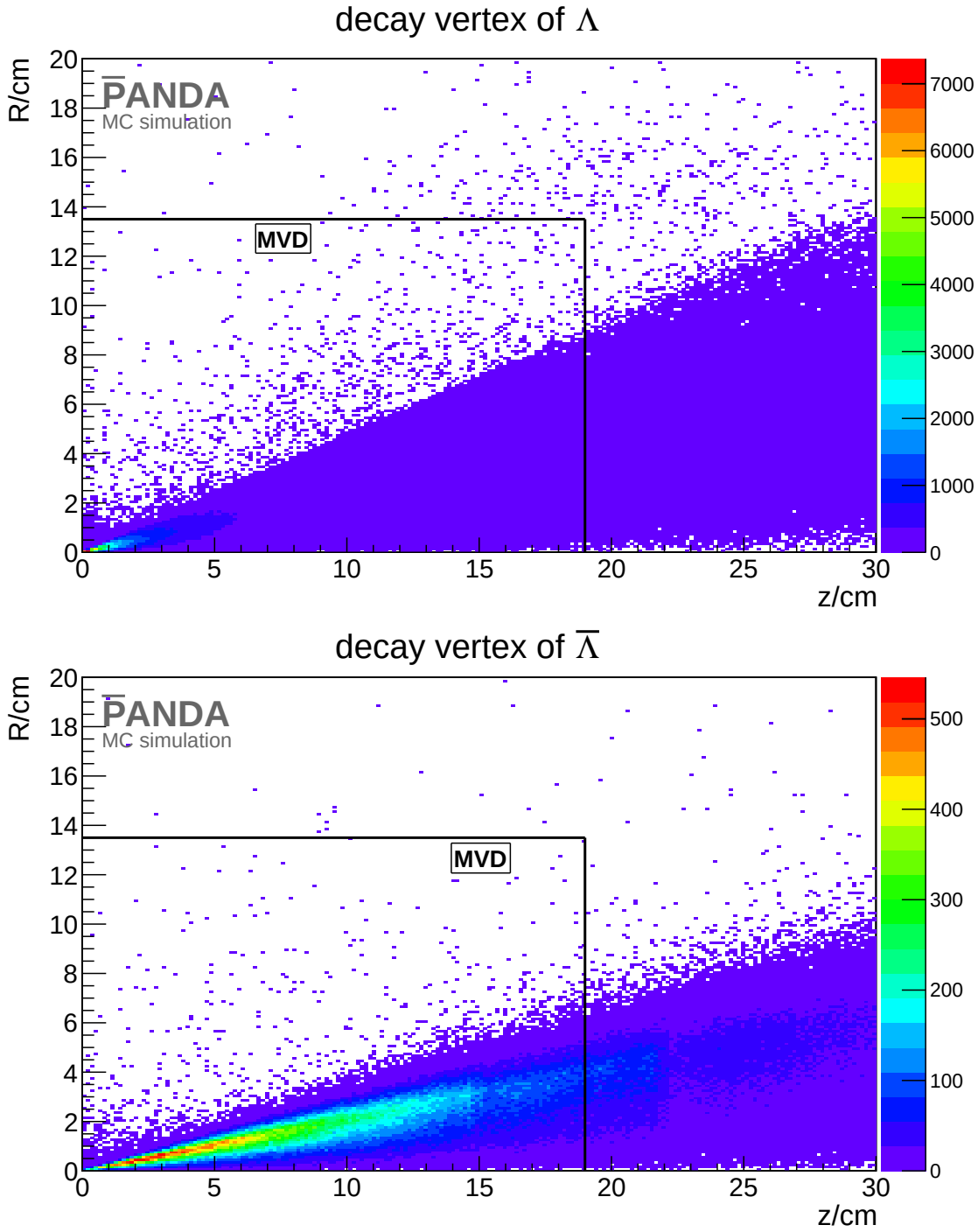

Figure 3.8: "PROPOSED FOR RELEASE" Decay vertex position of Λ (upper plot) and $\bar{\Lambda}$ (lower plot). In both plots the x axis shows the z coordinate (along the beam axis) of the decay vertex while the y axis shows its radial coordinate (the origin of the coordinate system s defined by the primary vertex). The black horizontal and vertical lines mark the radial and longitudinal extension of the MVD.

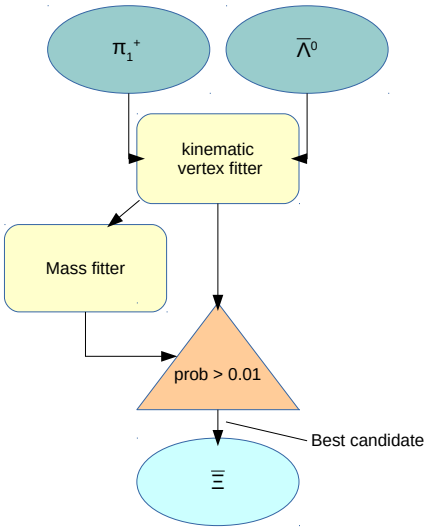

Figure 3.9: "PROPOSED FOR RELEASE" Scheme for $\bar{\Xi}^+$ reconstruction

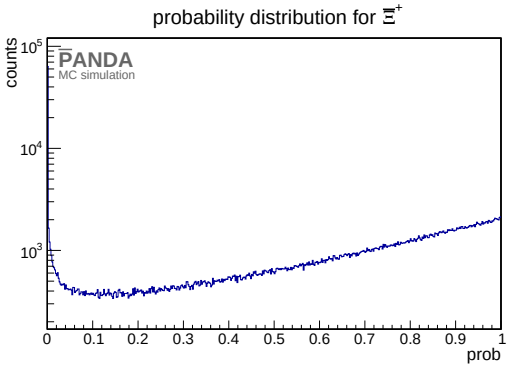

Figure 3.10: "PROPOSED FOR RELEASE" χ^2 probability for $\bar{\Xi}^+$ reconstruction

Table 3.3: "PROPOSED FOR RELEASE" Vertex resolution for $\bar{\Xi}^+$ and Ξ^- (charge conjugate. channel)

position	$\bar{\Xi}^+$	Ξ^- (from charge conjugate.)
x/cm	0.052	0.056
y/cm	0.052	0.052
z/cm	0.192	0.2

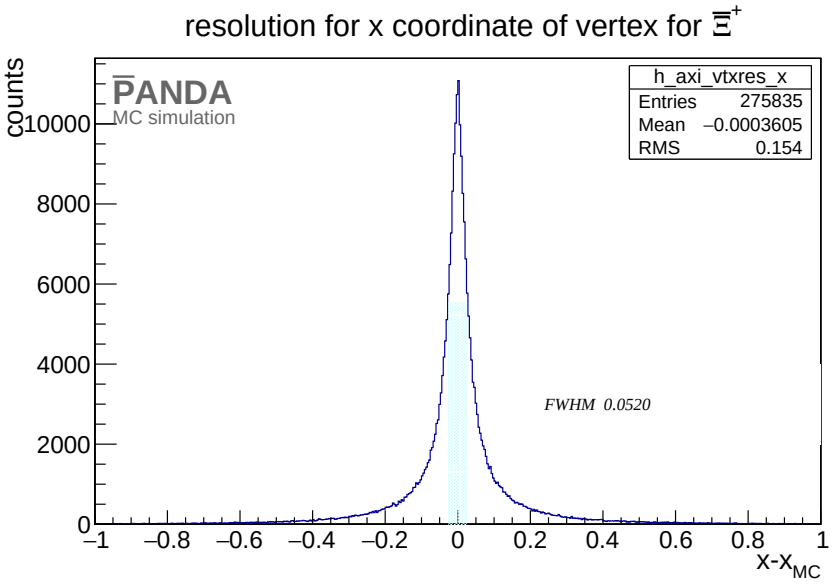

Figure 3.11: "PROPOSED FOR RELEASE" Vertex resolution of x position for $\bar{\Xi}^+$

Results

The vertex resolution after all cuts is shown in table 3.3.

It is determined by calculating the full width at half maximum (FWHM) of the distribution. The advantage of using this method for calculating the vertex resolution is that the FWHM is independent of distribution shape. Figure 3.11 and Figure 3.12 show the vertex resolution.

The mass distribution for the different cuts is shown in figure 3.13 and figure 3.14. The number of events is strongly reduced by the cut on the vertex fit probability. The width of the mass distribution gets smaller.

After using all cuts on the mass distribution the reconstructed mass of Ξ^- and $\bar{\Xi}^+$ can be determined by a double Gaussian fit. This is exemplarily shown for the Ξ^- in figure 3.15. The result of the mass fit is for $\bar{\Xi}^+$ m $= (1.32172 \pm 0.00396)$ GeV/c^2 and for Ξ^- m $= (1.3216 \pm 0.004)$ GeV/c^2. The two dimensional momentum distribution for $\bar{\Xi}^+$ and Ξ^- is shown in figure 3.16

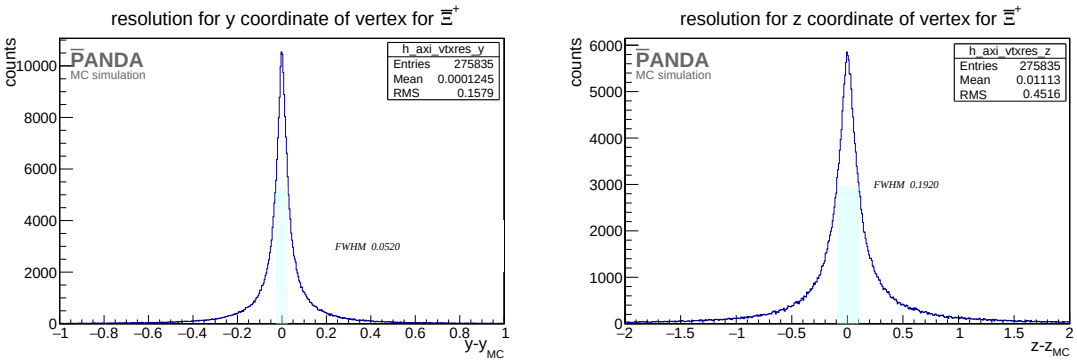

(a) Vertex resolution for y coordinate

(b) Vertex resolution for z coordinate

Figure 3.12: "PROPOSED FOR RELEASE" The left plot shows the vertex resolution of y position for $\bar{\Xi}^+$. The right plot shows the vertex resolution of z position for $\bar{\Xi}^+$.

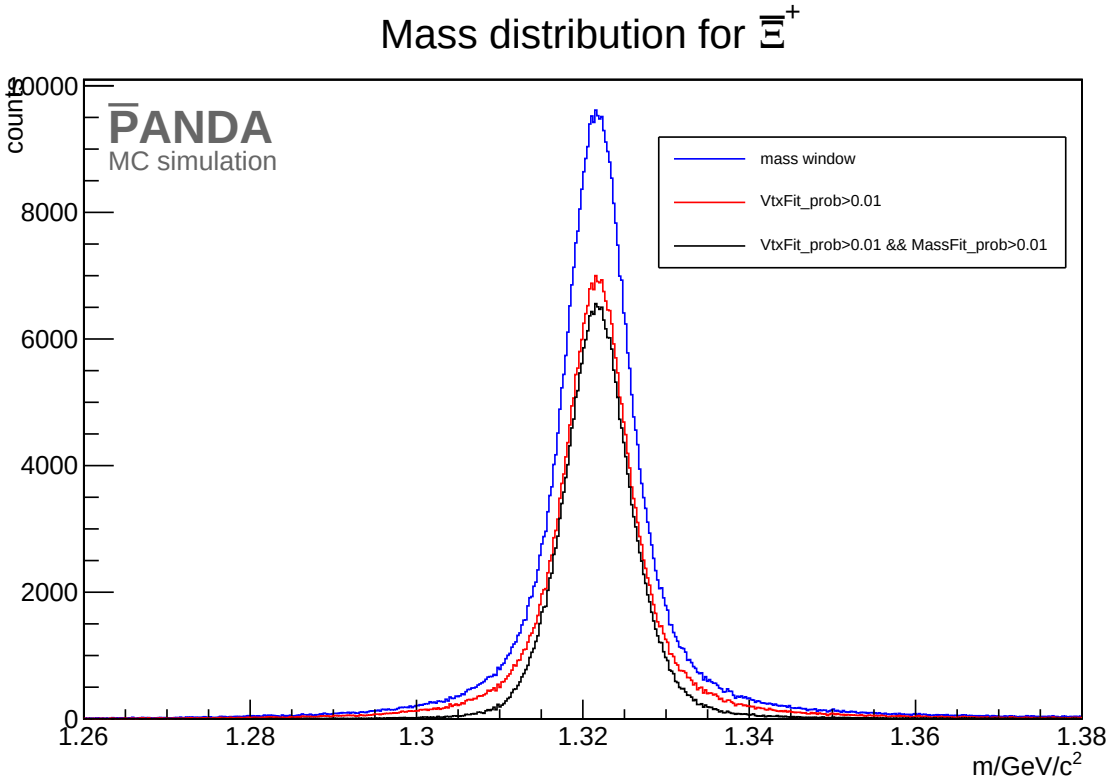

Figure 3.13: "PROPOSED FOR RELEASE" Mass distribution of $\bar{\Xi}^+$ for different cuts: the mass window cut is shown in blue, the vertex fit cut is shown in red and the distribution after all cuts is shown in black.

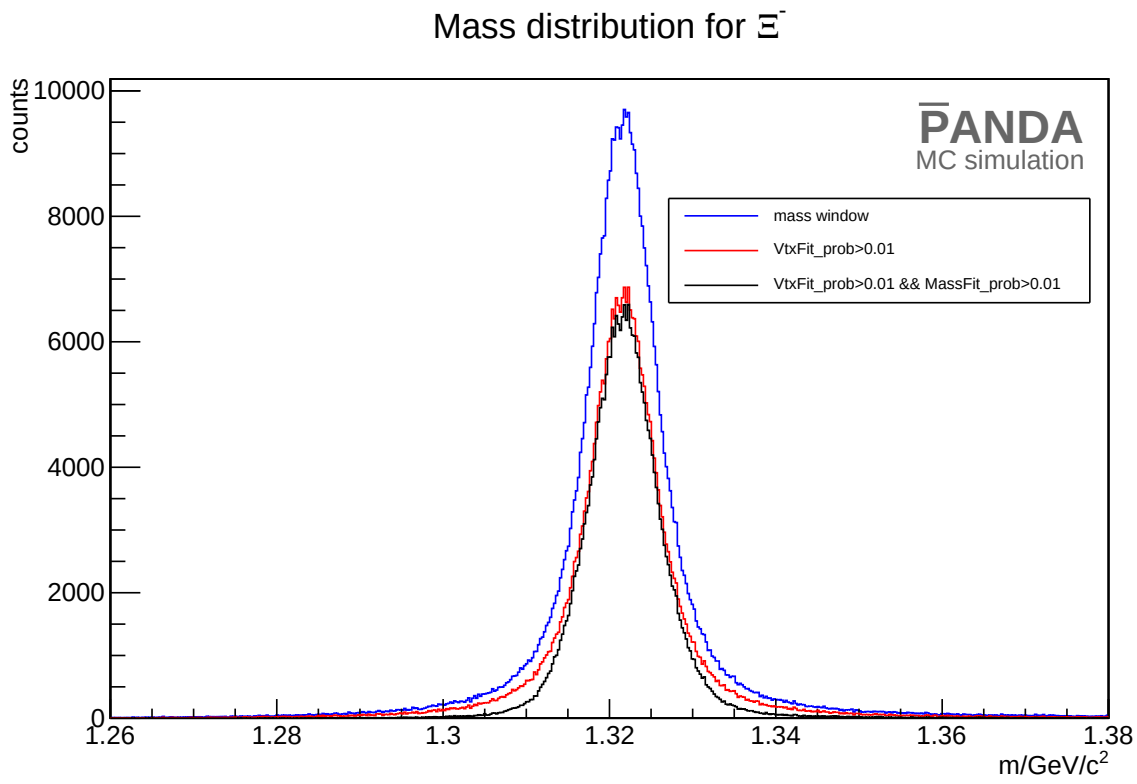

Figure 3.14: "PROPOSED FOR RELEASE" Mass distribution of Ξ^- for different cuts: mass window cut in blue, vertex fit cut in red and all cuts in black.

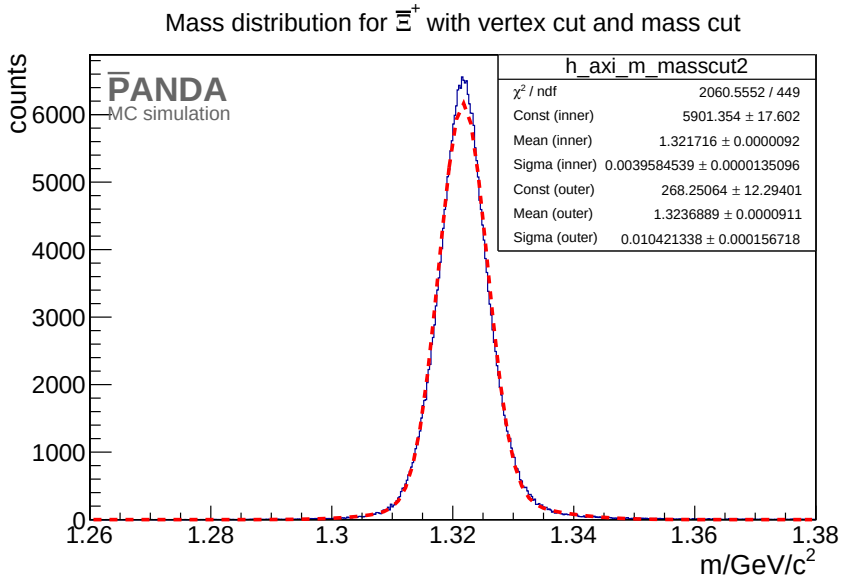

Figure 3.15: "PROPOSED FOR RELEASE" The plot shows the mass distribution (blue line) after all cuts. A double Gaussian fit (red dashed line) is performed to determine the reconstructed mass for the $\bar{\Xi}^+$.

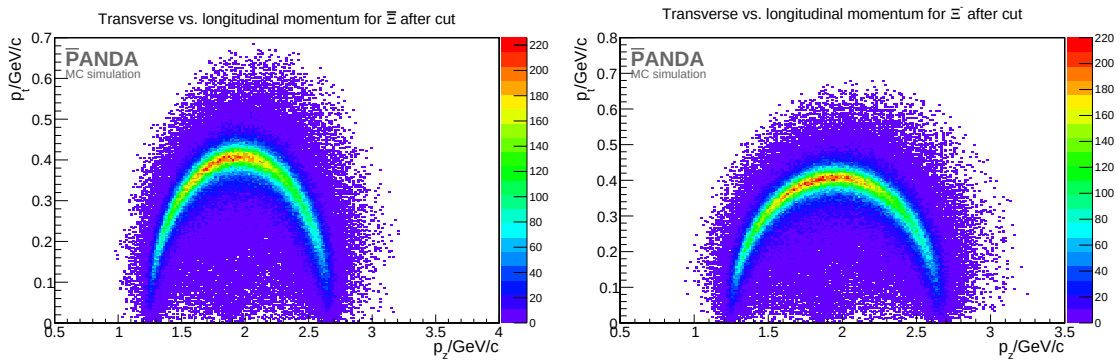

(a) $\bar{\Xi}^+$ (b) Ξ^-

Figure 3.16: "PROPOSED FOR RELEASE" The plots shows the transverse against the longitudinal momentum for $\bar{\Xi}^+$ and Ξ^-

Table 3.4: "PROPOSED FOR RELEASE" Vertex resolution for $\Xi^-(1820)$ and $\bar{\Xi}^+(1820)$.

position	$\Xi^-(1820)$	$\bar{\Xi}^+(1820)$ (from charge conjugate.)
x/cm	0.028	0.028
y/cm	0.028	0.028
z/cm	0.1	0.1

The reconstruction efficiency for $\bar{\Xi}^+$ is 18.39% and for Ξ^- 18.64%.

3.4 Reconstruction of $\Xi^-(1820)$ and $\bar{\Xi}^+(1820)$

Selection

For the reconstruction of $\Xi^-(1820)$ one combines Λ with the K^- meson and for $\bar{\Xi}^+(1820)$ $\bar{\Lambda}$ and K^+ using the best candidate from Λ and $\bar{\Lambda}$. After the combination of the particles a mass window cut with width of $0.3\,\mathrm{GeV/c^2}$ is performed. The daughter particles are fitted then to a common vertex point with the PndKinVtxFitter. Only those candidates for $\Xi^-(1820)$ ($\bar{\Xi}^+(1820)$) are selected which have a fit probability of more then 1%. The selection scheme is shown in figure 3.17.

The χ^2 probability distribution for the vertex fit is shown in figure 3.18. The distribution is again not flat but increases for values up to one.

If there is more than one particle the best candidate is chosen.

Results

The vertex resolution for $\Xi^-(1820)$ and $\bar{\Xi}^+(1820)$ is summarized in table 3.4.

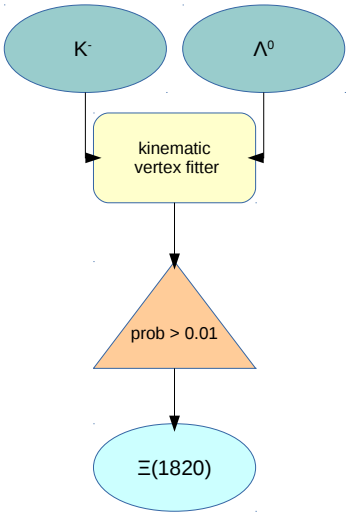

Figure 3.17: "PROPOSED FOR RELEASE" Scheme for $\Xi^-(1820)$ reconstruction

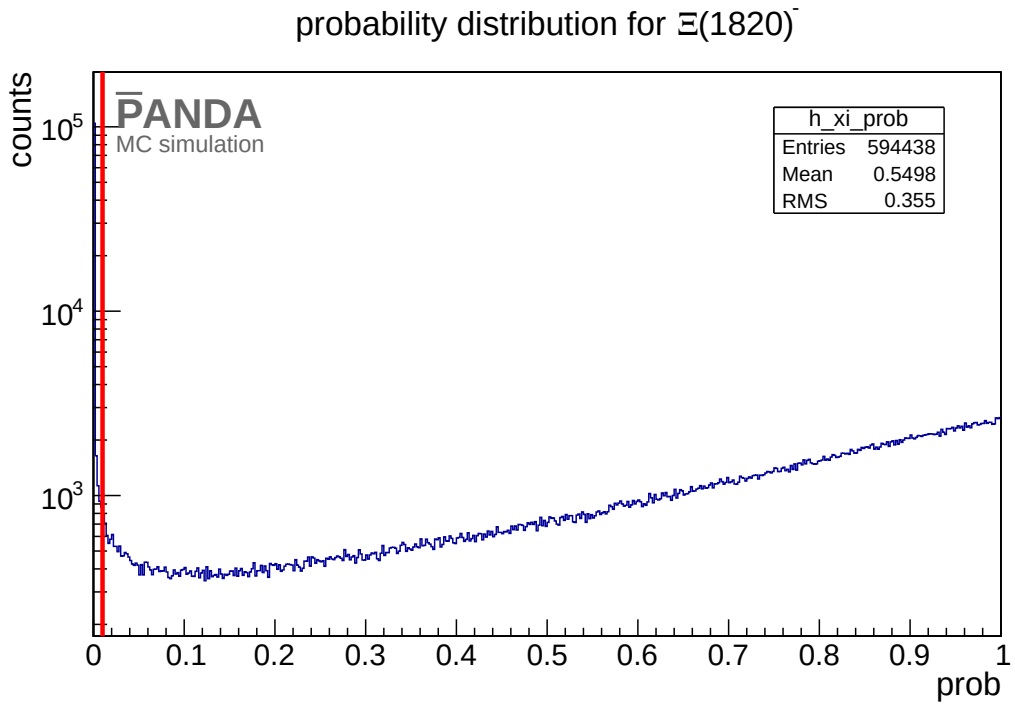

Figure 3.18: "PROPOSED FOR RELEASE" χ^2 probability distribution of kinematic vertex fit for Ξ^- (1820).

Here again the vertex resolution is calculated with the FWHM. This is exemplarily shown for Ξ^- (1820) in figure 3.19 and figure 3.20.

After performing both fits and cut on the probability values, the mass for Ξ^- (1820) and $\bar{\Xi}^+$ (1820) can be determined by fitting with a double Gaussian function. Figure 3.21 shows the mass distribution for both particles after each cut.

The mass fit is exemplarily shown for the Ξ^- (1820) in figure 3.22.

The mass value for the Ξ^- (1820) is fitted to $m_{\Xi^*} = 1.8229 \pm 3.81 \cdot 10^{-5}$ GeV/c^2 and for $\bar{\Xi}^+$ (1820) to $m_{\bar{\Xi}^*} = 1.823 \pm 3.73 \cdot 10^{-5}$ GeV/c^2. These values are close to the input value. Figure 3.23 shows the two dimensional momentum distribution. For both subplots the x axis shows the longitudinal momentum and on the y axis there is shown the transverse momentum.

The reconstructed distributions are in good agreement with the distribution coming from the simulated events which are shown in figure 2.3 (b).

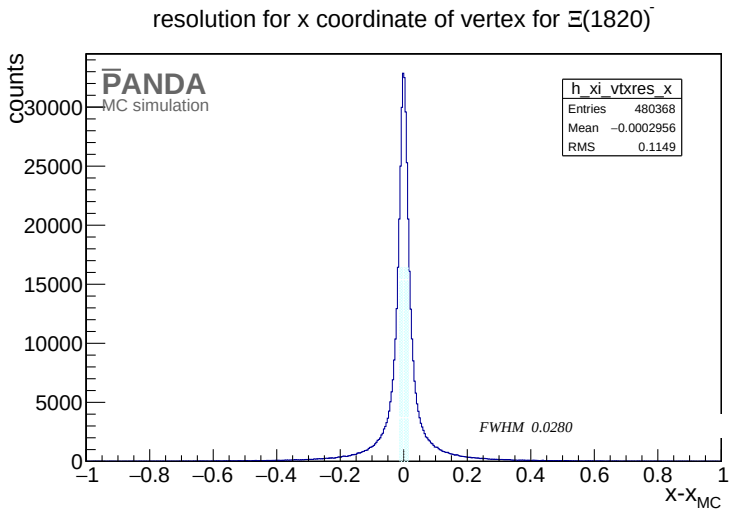

Figure 3.19: "PROPOSED FOR RELEASE" Vertex resolution of the x coordinate for Ξ^- (1820).

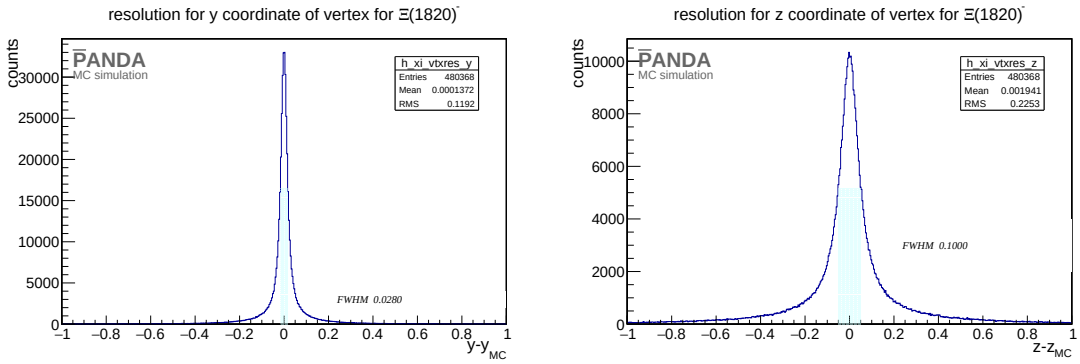

(a) Vertex resolution of the y coordinate for Ξ^- (1820). (b) Vertex resolution of the z coordinate for Ξ^- (1820).

Figure 3.20: "PROPOSED FOR RELEASE" Figure a) shows the vertex resolution for the y coordinate and figure b) for the z coordinate of Ξ^- (1820)

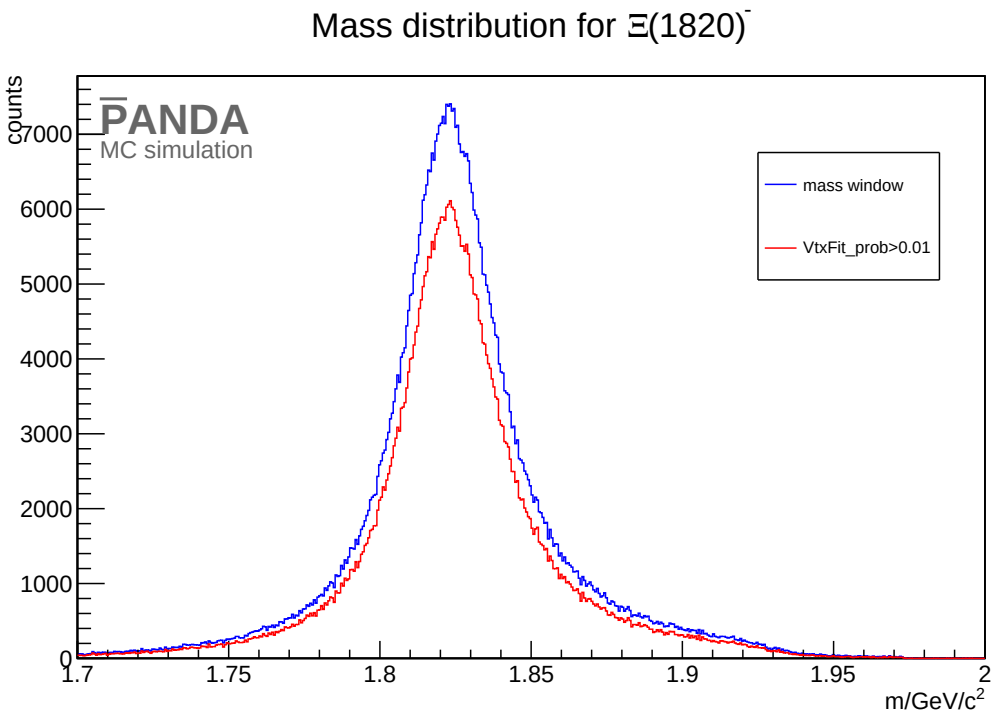

Figure 3.21: "PROPOSED FOR RELEASE" Mass distribution for Ξ^- (1820) after the mass window cut in blue and after the vertex fit probability cut in red.

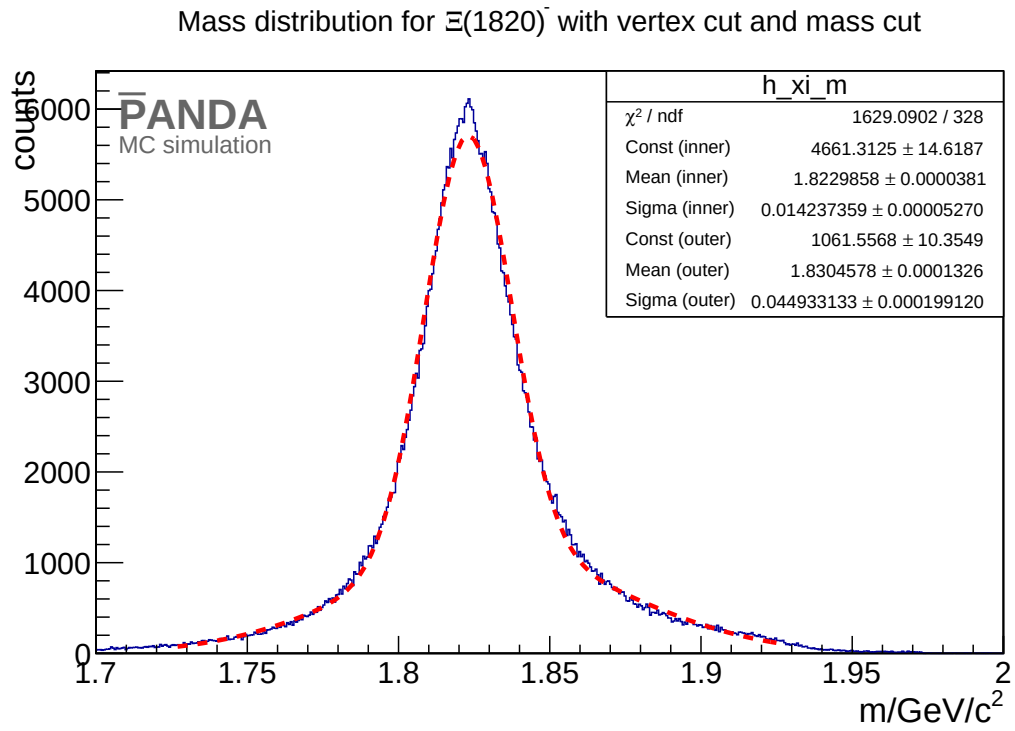

Figure 3.22: "PROPOSED FOR RELEASE" Mass distribution (blue line) after all cuts for Ξ^- (1820). The performed double Gaussian fit is shown as red dashed line.

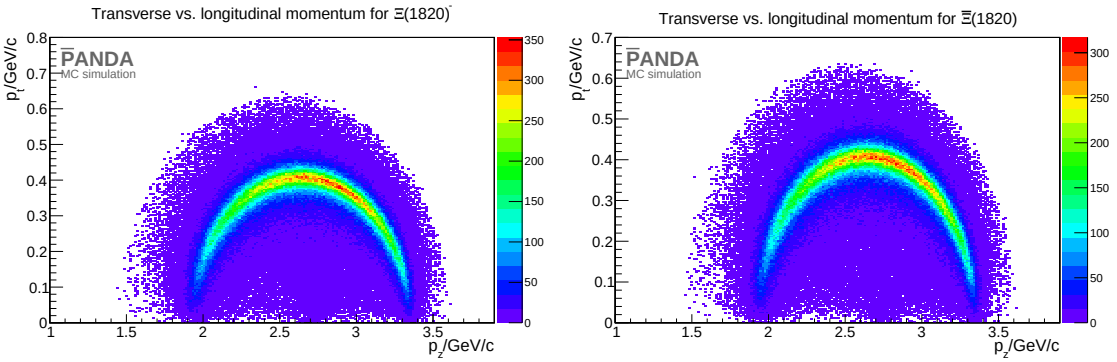

(a) Ξ^- (1820) (b) $\bar{\Xi}^+$ (1820)

Figure 3.23: "PROPOSED FOR RELEASE" Both plots show the longitudinal versus the transverse momentum of the excited cascade baryon.

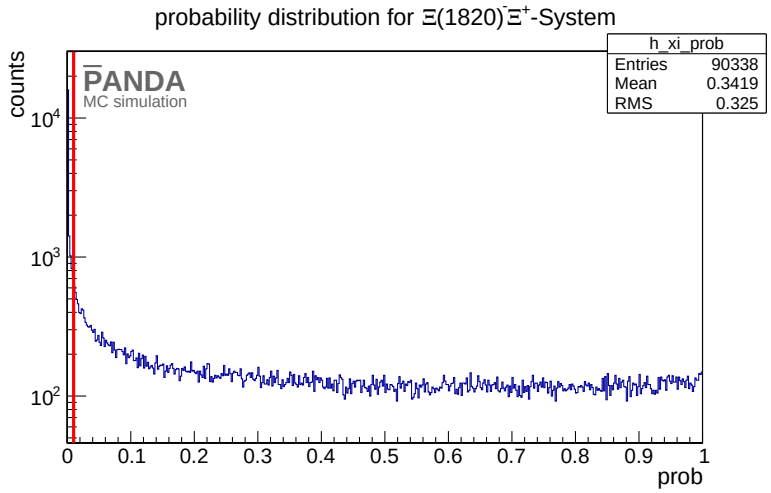

Figure 3.24: "PROPOSED FOR RELEASE" 4-constraint fit probability. The red line denotes the cut value of 1%.

3.5 Reconstruction of the whole reaction chain

Selection

To reconstruct the whole reaction chain Ξ^- (1820) and $\bar{\Xi}^+$ are combined. This is also done with $\bar{\Xi}^+$ (1820) and Ξ^- for the charge conjugated channel. For this reconstruction the event selection is done with an exclusive method. The resulting four-momentum vector of both daughter particles – here Ξ^- (1820) and $\bar{\Xi}^+$ and there charge conjugate. particles – is fitted with the constraint to match to the initial for momentum vector

$$\left(\mathrm{p}_x,\, \mathrm{p}_y,\, \mathrm{p}_z,\, \mathrm{E}\right) = (0,\, 0,\, 4.6,\, 5.63)$$

of the $\bar{\mathrm{p}}\mathrm{p}$. This fit is performed with the PndKinFitter. After the four-momentum fit only those candidates are selected which have a χ^2 probability of more than 1%. The χ^2 probability is shown in figure 3.24. The red line denotes the cut value.
The selection scheme is shown in figure 3.25

Results

The results of the reconstruction efficiency for all non-final state particles is shown in table 3.5 and table 3.6.
Figure 3.26 shows the Dalitz plot for the $\bar{\Xi}^+$, Λ and K^- final states after the reconstruction. Compared with the Dalitz plot of the simulated particles shown in figure 2.4 the

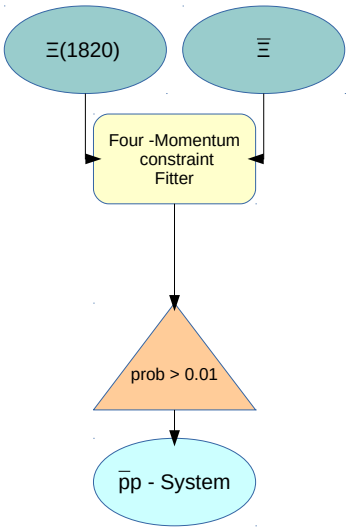

Figure 3.25: "PROPOSED FOR RELEASE" Scheme for the reconstruction of the whole reaction chain.

Table 3.5: "PROPOSED FOR RELEASE" reconstruction efficiency for non-final state particles for $\bar{p}p \rightarrow \Xi^- (1820)\ \bar{\Xi}^+$

particle	reco. efficiency in %	dp/p in %
Λ	50.33	1.50
$\bar{\Lambda}$	41.46	1.45
$\bar{\Xi}^+$	18.39	1.29
$\Xi^- (1820)$	32.02	2.68
$\Xi^- (1820)\ \bar{\Xi}^+$ system	4.69	1.03

Table 3.6: "PROPOSED FOR RELEASE" reconstruction efficiency for non-final state particles for $\bar{p}p \rightarrow \bar{\Xi}^+ (1820)\ \Xi^-$

particle	reco. efficiency in %	dp/p in %
Λ	42.47	1.45
$\bar{\Lambda}$	49.0	1.50
Ξ^-	18.64	2.30
$\bar{\Xi}^+ (1820)$	33.22	1.31
$\bar{\Xi}^+ (1820)\ \Xi^-$ system	4.87	1.03

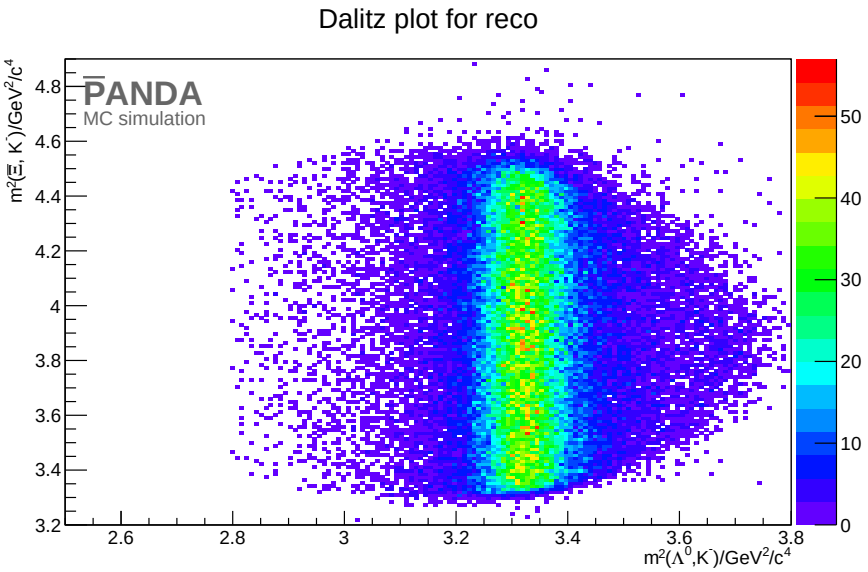

Figure 3.26: "PROPOSED FOR RELEASE" Dalitz plot for reconstructed particles

171 reconstruction seems to be good.

4 Background

For background studies 15 million events are simulated with the Dual Parton Model based generator DPM. To make the selected events of background and signal comparable a scaling factor is needed. This scaling factor can be calculated with the number of generated events and the cross section of signal and background.

$$B = \frac{N_{\text{sig}}/\left(\sigma_{\text{sig}}\right)}{N_{\text{bg}}/\sigma_{\text{bg}}}, \tag{4.0.1}$$

where N_{sig} is the number of generated signal events and N_{bg} the number of generated background events. The cross section are given by $\sigma_{\text{sig}} = 1\,\mu\text{b}$ and $\sigma_{\text{bg}} = 50\,\text{mb}$ [1]. The scaling factor for the channel $\bar{\text{p}}\text{p} \to \Xi^-\,(1820)\;\bar{\Xi}^+$ is $B = 5000$. The scaling factor for the c.c. channel is the same.

All background events are reconstructed like the signal events. The number of reconstructed Background events is shown in table 4.1.

Multiplying the number of background events with the scaling factor make them comparable with the number of signal events. The comparison between signal and background events is shown in table 4.2. The significance is given by

$$S = \frac{N_{\text{sig}}^2}{N_{\text{sig}} + N_{\text{bg}}}, \tag{4.0.2}$$

where N_{bg} is scaled with B.

Because there are no background events left, it is only possible to estimate a upper limit for the significance. For one background event which is scaled with B the significance is

Table 4.1: Number of reconstructed background events for $\bar{\text{p}}\text{p} \to \Xi^-\,(1820)\;\bar{\Xi}^+$

Particle	N_{bg}
Λ	264,142
$\bar{\Lambda}$	124,068
$\bar{\Xi}^+$	3,062
$\Xi^-\,(1820)$	298
$\Xi^-\,(1820)\;\bar{\Xi}^+$	0

Table 4.2: "PROPOSED FOR RELEASE" The number of background events scaled with B compared to the number of signal events for $\bar{p}p \rightarrow \Xi^-(1820)\,\bar{\Xi}^+$. The significance is calculated with equation 4.0.2.

Particle	N_{sig}	$N_{bg} \cdot B$	S
Λ	786,243	$1.321 \cdot 10^9$	467.68
$\bar{\Lambda}$	711,820	$620.341 \cdot 10^6$	815.85
$\bar{\Xi}^+$	302,681	$15.31 \cdot 10^6$	5,868.03
$\Xi^-(1820)$	490,672	$1.49 \cdot 10^6$	121,544.21
$\Xi^-(1820)\,\bar{\Xi}^+$	74,523	0	$<$ 69,837.37

less than 69,837.37. Further background studies for this reaction chain and its charged conjugated channel have to be done as a next step.

5 Summary and Conclusion

The hole reaction chain can be reconstructed with an efficiency of nearly 5% for both channels.
Final states particles have a reconstruction efficiency of nearly 80%. The reconstruction of Λ and $\bar{\Lambda}$ shows a difference in the efficiencies. This is caused by the different mother particles of the Λ and $\bar{\Lambda}$. The reconstruction efficiency for Λ and $\bar{\Lambda}$ might be improved by using lambda discs. But this has to be check and is one of the next steps in this analysis.
The reconstructed mass for $\Xi^{-}\,(1820)$ and $\bar{\Xi}^{+}\,(1820)$ is in a good agreement with the literature value coming from [3].
The topology of the decay chain suppresses the background efficiently. The comparison between the number of signal and background events shows how good background events could be suppressed by the selection. After the reconstruction of the hole reaction chain the number of simulated signal events is 74,523 and the number of background events is 0. Assuming one background event gives a limit for the significance of $S < 69,837.37$. To make a more pricise statement more background simulation is needed.

References

[1] W. Erni, I. Keshelashvili, B. Krusche, M. Steinacher, Y. Heng, Z. Liu, H. Liu, X. Shen, O. Wang, H. Xu, *et al.*, "Physics performance report for panda: Strong interaction studies with antiprotons," *arXiv preprint arXiv:0903.3905*, 2009.

[2] V. Flaminio, W. G. Moorhead, D. R. O. Morrissson, and N. Rivoire, "Cern report no. cern-hera84-01." (unpublished), 1984.

[3] J. B. et al., *Particle Data Group.* Phys. Rev. D86, 010001, 2012.

[4] R. Kliemt. private communication, 2015.